mathematics

MDPI

Article

Buckling Analysis of Functionally Graded Tapered Microbeams via Rayleigh–Ritz Method

Bekir Akgöz [1,*] and Ömer Civalek [1,2]

[1] Division of Mechanics, Department of Civil Engineering, Akdeniz University, Antalya 07070, Turkey
[2] Department of Medical Research, China Medical University Hospital, China Medical University, Taichung 404, Taiwan
* Correspondence: bekirakgoz@akdeniz.edu.tr

Abstract: In the present study, the buckling problem of nonhomogeneous microbeams with a variable cross-section is analyzed. The microcolumn considered in this study is made of functionally graded materials in the longitudinal direction and the cross-section of the microcolumn varies continuously throughout the axial direction. The Bernoulli–Euler beam theory in conjunction with modified strain gradient theory are employed to model the structure by considering the size effect. The Rayleigh–Ritz numerical solution method is used to solve the eigenvalue problem for various conditions. The influences of changes in the cross-section and Young's modulus, size dependency, and non-classical boundary conditions are examined in detail. It is observed that the size effect becomes more pronounced for smaller sizes and differences between the classical and non-classical buckling loads increase by increasing the taper ratios.

Keywords: size effect; Rayleigh–Ritz method; buckling; modified strain gradient theory; tapered microcolumn

MSC: 65L15; 65L60; 74K10; 74M25

Citation: Akgöz, B.; Civalek, Ö. Buckling Analysis of Functionally Graded Tapered Microbeams via Rayleigh–Ritz Method. *Mathematics* **2022**, *10*, 4429. https://doi.org/10.3390/math10234429

Academic Editor: Fernando Simoes

Received: 25 October 2022
Accepted: 23 November 2022
Published: 24 November 2022

1. Introduction

Engineering is a profession in which the principles of nature are applied to create useful objects. A mechanical engineer develops a new engine. A mechatronic engineer designs a robot. Civil engineers design a bridge, a dam, or a building. An electronic engineer designs a computer or an integrated circuit. For many reasons, an engineer is not only interested in a design that works at a nominal level but also one which is somehow the best design. Simply put, the process of determining the best design is called optimization. Consequently, we may wish to design the lowest-cost bridge for the site.

On the other hand, it is not always possible or economical to design and build structures/prismatic structures with one-type (homogeneous) of, or a constant, cross-section. For this reason, it is useful to use two or more materials with variable cross-sections in many engineering applications.

Functionally graded materials (FGMs) can be described as relatively new types of composite materials that are used in various engineering applications, such as turbine blades, cutting tools, rocket bodies, engine cylinders, artificial bones, and dental implants. Due to the gradual and smooth variation of their material properties, FGMs have some desired properties, for example, in avoiding cracking and delamination problems and diminishing undesired stress concentrations between laminates. These improved materials were introduced by a group of Japanese scientists in 1984 to propose a thermal barrier material that can withstand a surface temperature of 2000 °K and a temperature range of 1000 °K for a section thinner than 10 mm in aircrafts and space shuttles [1].

With rapid developments in technology, FGMs have recently been applied in micro-/nano-electromechanical systems (MEMS/NEMS), for example, as a structural element in

shape memory alloy films [2], electrically actuated MEMS devices [3], and atomic force microscopes [4]. The characteristic dimensions of these microstructures are specified in micrometers and/or nanometers. As has been demonstrated through experimentation, the size effect phenomenon plays a key role in the mechanical characteristics of microstructures [5–12]. Experimental studies to determine the static and dynamic behaviors of structural elements are very important and valid. However, testing these structures under different conditions is very laborious, expensive, and not feasible, especially at the micro and nanoscales.

Solid mechanics is a branch of continuum mechanics that deals with the static and dynamic responses of structures by modelling them mathematically. The mathematical modelling of structures can be simpler, cheaper, and more useful than experimental works. Consequently, continuum mechanics may be considered as a potential approach to determine the mechanical behaviors of small-sized structures. Unfortunately, classical continuum theory fails to estimate the responses of microstructures due to inability to consider the size effect phenomena. Thus, the utilization of size-dependent theories containing at least one material length scale parameter is required. Several higher-order elasticity theories have been proposed such as couple stress, nonlocal elasticity, strain gradient, nonlocal strain gradient, and doublet mechanics theories [13,14]. These theories have been frequently employed to analyze microstructures in the past [15–30].

Free vibration and buckling behaviors of axially functionally graded (AFG) tapered beams were numerically investigated by utilizing differential quadrature [31], differential transform [32], and direct integral methods [33]. The transverse vibration of functionally graded thick beams was examined using the Timoshenko beam theory [34] and a refined beam theory considering thickness-stretching effect [35]. The interpolation matrix method was applied to obtain the critical buckling loads of AFG-tapered thick beams based on the first-order shear deformation beam theory [36]. A general solution for the free vibration of AFG-tapered cantilevers with a tip mass was presented based using the Bernoulli–Euler beam theory and the Myklestad method [37]. The thermo-mechanical buckling of bi-directional functionally graded porous microbeams was studied [38]. Material properties were changed throughout the height and length of the microbeam according to the power law. The free vibrational response of non-prismatic AFG Timoshenko beams were subjected to thermal variation in humid environments and examined via the harmonic differential quadrature method [39].

Size-dependent stability analysis of homogeneous microbeams with varying cross-sections was carried out based on the Bernoulli–Euler beam theory and modified strain gradient theory [40]. Moreover, the buckling response of Bernoulli–Euler AFG-tapered microstructures was examined using a modified couple stress theory for different boundary conditions [41]. Nonlocal strain gradient theory was used to model the buckling response of AFG nanobeams lying on a variable elastic foundation [42]. An analytical solution for the static and dynamic responses of functionally graded tapered microbridges was introduced on the basis of modified couple stresses and three-dimensional beam theories [43]. Stability and free vibration responses of tapered functionally graded composite microbeams reinforced by carbon nanotube were subjected to a magnetic field and investigated using the finite element method [44]. The free vibration of viscoelastic tapered microbars embedded in a visco-Pasternak foundation was studied based on strain gradient theory and the Kelvin–Voigt model [45]. Size-dependent nonlinear vibrations of functionally graded microbeams with porosities was carried out based on modified couple stress and Bernoulli–Euler beam theories. The numerical results were obtained by utilizing generalized differential quadrature and direct iterative methods [46]. A buckling analysis of bi-directional functionally graded tapered Bernoulli–Euler porous nanobeams was performed via nonlocal elasticity theory [47]. Moreover, the thermo-mechanical vibrational response of rotary functionally graded tapered Bernoulli–Euler nanobeams was perused for cantilever and propped cantilever beams on the basis of nonlocal elasticity theory [48].

From this literature survey, it can be seen that there are many studies on the linear and nonlinear mechanical behaviors of functionally graded tapered micro and nanobeams based on nonlocal elasticity, modified couple stress, and nonlocal strain gradient theories in particular. To the best of the authors' knowledge, there is no study on the size-dependent buckling analysis of axially functionally graded tapered microstructures based on the modified strain gradient theory by considering higher-order boundary conditions and by possessing variable length scale parameters. In this work, microstructure-dependent buckling of AFG-tapered microbeams is examined. Euler-Bernoulli beam and modified strain gradient theories are utilized to formulate the AFG-tapered microbeams. The Rayleigh–Ritz method is applied to obtain the critical buckling loads of cantilever and propped cantilever microbeams at various taper ratios and gradient indices. Effects of taper ratios, material property gradient indices, length scale parameters, and nonclassical boundary conditions are investigated in detail.

2. Theory and Formulation

Modified strain gradient theory (SGT) is introduced by Lam et al. [5]. This nonclassical elasticity theory includes three additional material length scale parameters to take into consideration when investigating size effect. According to this theory, the strain energy U in a linear elastic isotropic material can be expressed as

$$U = \frac{1}{2}\int_0^L \int_A \left(\sigma_{ij}\varepsilon_{ij} + p_i\gamma_i + \tau_{ijk}^{(1)}\eta_{ijk}^{(1)} + m_{ij}^s\chi_{ij}^s\right) dA dx \tag{1}$$

$$\varepsilon_{ij} = \frac{1}{2}\left(u_{i,j} + u_{j,i}\right) \tag{2}$$

$$\varepsilon_{mm,i} = \gamma_i \tag{3}$$

$$\begin{aligned}\eta_{ijk}^{(1)} = {} & \tfrac{1}{3}\left(\varepsilon_{jk,i} + \varepsilon_{ki,j} + \varepsilon_{ij,k}\right) - \tfrac{1}{15}\left[\left(\delta_{ij}(\varepsilon_{mm,k} + 2\varepsilon_{mk,m})\right.\right. \\ & \left.\left. + \delta_{jk}(\varepsilon_{mm,i} + 2\varepsilon_{mi,m}) + \delta_{ki}\left(\varepsilon_{mm,j} + 2\varepsilon_{mj,m}\right)\right)\right]\end{aligned} \tag{4}$$

$$\chi_{ij}^{(s)} = \frac{1}{2}\left(\theta_{i,j} + \theta_{j,i}\right) \tag{5}$$

$$\theta_i = \frac{1}{2}e_{ijk}u_{k,j} \tag{6}$$

where u_i, θ_i, ε_{ij}, γ_i, $\eta_{ijk}^{(1)}$, and χ_{ij}^s represent the components of the displacement and rotation vectors, the classical strain tensor, the dilatation gradient vector, the deviatoric stretch gradient, and the symmetric rotation gradient tensors, respectively. δ is Kronecker delta and e_{ijk} is an alternate symbol. Furthermore, the components of the classical stress tensor and the higher-order stress tensors can be defined as [5]

$$\sigma_{ij} = \lambda\varepsilon_{mm}\delta_{ij} + 2G\varepsilon_{ij} \tag{7}$$

$$p_i = 2Gl_0^2\gamma_i \tag{8}$$

$$\tau_{ijk}^{(1)} = 2Gl_1^2\eta_{ijk}^{(1)} \tag{9}$$

$$m_{ij}^s = 2Gl_2^2\chi_{ij}^s \tag{10}$$

where l_0, l_1, l_2 are the additional material length scale parameters. λ and G are the Lamé constants and can be defined in terms of Young's modulus and Poisson's ratio as

$$\lambda = \frac{Ev}{(1+v)(1-2v)} \tag{11}$$

$$G = \frac{E}{2(1+v)} \tag{12}$$

The displacement components of an initially straight Bernoulli–Euler beam can be defined as

$$u(x,z) = -z\frac{\mathrm{d}w(x)}{\mathrm{d}x} \tag{13}$$

$$v(x,z) = 0 \tag{14}$$

$$w(x,z) = w(x) \tag{15}$$

where u, v, and w are the components of the displacement vector in $x-$, $y-$, and $z-$ axes, respectively. Using Equations (13)–(15) in Equations (2)–(5) yields the following nonzero components of the classical and higher-order strains as

$$\varepsilon_{xx} = -z\frac{\mathrm{d}^2w}{\mathrm{d}x^2} \tag{16}$$

$$\gamma_x = -z\frac{\mathrm{d}^3w}{\mathrm{d}x^3} \tag{17}$$

$$\gamma_z = -\frac{\mathrm{d}^2w}{\mathrm{d}x^2} \tag{18}$$

$$\eta^{(1)}_{xxx} = -\frac{2}{5}\left(z\frac{\mathrm{d}^3w}{\mathrm{d}x^3}\right) \tag{19}$$

$$\eta^{(1)}_{xxz} = \eta^{(1)}_{xzx} = \eta^{(1)}_{zxx} = -\frac{4}{15}\left(\frac{d^2w}{dx^2}\right) \tag{20}$$

$$\eta^{(1)}_{xyy} = \eta^{(1)}_{xzz} = \eta^{(1)}_{yxy} = \eta^{(1)}_{yyx} = \eta^{(1)}_{zxz} = \eta^{(1)}_{zzx} = \frac{1}{5}\left(z\frac{\mathrm{d}^3w}{\mathrm{d}x^3}\right) \tag{21}$$

$$\eta^{(1)}_{yyz} = \eta^{(1)}_{yzy} = \eta^{(1)}_{zyy} = \frac{1}{15}\left(\frac{d^2w}{dx^2}\right) \tag{22}$$

$$\eta^{(1)}_{zzz} = \frac{1}{5}\left(\frac{\mathrm{d}^2w}{\mathrm{d}x^2}\right) \tag{23}$$

$$\chi^{s}_{xy} = \chi^{s}_{yx} = -\frac{1}{2}\left(\frac{d^2w}{dx^2}\right) \tag{24}$$

By substituting Equations (16)–(24) into Equations (7)–(10), the nonzero components of macro and micro stresses can be obtained as (by neglecting Poisson effect [29])

$$\sigma_{xx} = -Ez\frac{\mathrm{d}^2w}{\mathrm{d}x^2} \tag{25}$$

$$p_x = -2Gl_0^2z\frac{\mathrm{d}^3w}{\mathrm{d}x^3} \tag{26}$$

$$p_z = -2Gl_0^2\frac{d^2w}{\mathrm{d}x^2} \tag{27}$$

$$\tau^{(1)}_{xxx} = -\frac{4}{5}Gl_1^2z\frac{\mathrm{d}^3w}{dx^3} \tag{28}$$

$$\tau^{(1)}_{xxz} = \tau^{(1)}_{xzx} = \tau^{(1)}_{zxx} = -\frac{8}{15}Gl_1^2\frac{d^2w}{\mathrm{d}x^2} \tag{29}$$

$$\tau^{(1)}_{xyy} = \tau^{(1)}_{xzz} = \tau^{(1)}_{yxy} = \tau^{(1)}_{yyx} = \tau^{(1)}_{zxz} = \tau^{(1)}_{zzx} = \frac{2}{5}Gl_1^2z\frac{\mathrm{d}^3w}{dx^3} \tag{30}$$

$$\tau^{(1)}_{yyz} = \tau^{(1)}_{yzy} = \tau^{(1)}_{zyy} = \frac{2}{15}Gl_1^2\frac{d^2w}{\mathrm{d}x^2} \tag{31}$$

$$\tau_{zzz}^{(1)} = \frac{2}{5} G l_1^2 \frac{d^2 w}{dx^2} \tag{32}$$

$$m_{xy}^s = m_{yx}^s = -G l_2^2 \frac{d^2 w}{dx^2} \tag{33}$$

Using above equations into Equation (1) yields an expression for the strain energy U as

$$U = \frac{1}{2} \int_0^L \left[\left(EI + GA \left(2l_0^2 + \frac{8}{15} l_1^2 + l_2^2 \right) \right) \left(\frac{d^2 w}{dx^2} \right)^2 + \left(GI \left(2l_0^2 + \frac{4}{5} l_1^2 \right) \right) \left(\frac{d^3 w}{dx^3} \right)^2 \right] dx \tag{34}$$

where A and I are the cross-section and second moment of area, respectively.

3. Buckling of an AFG-Tapered Microcolumn

In the present study, it is considered that the cross-section $A_{(x)}$ and second moment of area $I_{(x)}$ are linearly varied along the longitudinal direction. Moreover, the material properties of Young's modulus $E_{(x)}$, the shear modulus $G_{(x)}$, and the length scale parameters $l_{i_{(x)}}$ change gradually in this direction. They can be described as

$$A(x) = A_L \left(1 - \alpha \frac{x}{L} \right) \tag{35}$$

$$I_{(x)} = I_L \left(1 - \alpha \frac{x}{L} \right) \tag{36}$$

$$E_{(x)} = E_L + (E_R - E_L) V_R \tag{37}$$

$$G_{(x)} = G_L + (G_R - G_L) V_R \tag{38}$$

$$l_{i_{(x)}} = l_{i_L} + \left(l_{i_R} - l_{i_L} \right) V_R \ (i = 0, 1, 2) \tag{39}$$

where α represents the taper ratio, and the subscripts L and R denote left and right sides of the microbeam, respectively. V_R defines the volume fraction of the right side's material equals $\left(\frac{x}{L} \right)^n$ in which n is the non-negative material property gradient index. It is notable that if $\alpha = 0$, the microbeam will have a uniform section. On the other hand, if $n = 0$ *or* ∞, the microbeam will be homogeneous. Variation of the volume fraction of right side's material throughout the longitudinal direction for various gradient indices is depicted in Figure 1. It is seen from this figure that V_R becomes bigger for lower values of the material property gradient index and approaches to zero by increasing the material property gradient index.

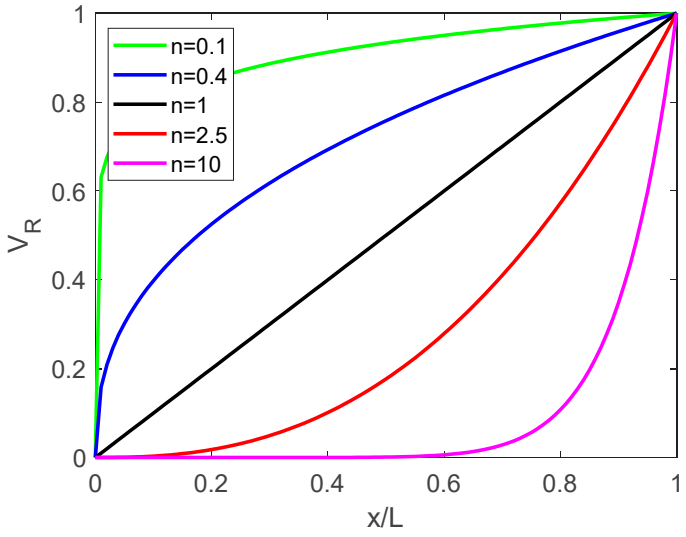

Figure 1. Variation of V_R throughout the longitudinal direction for various gradient indices.

The strain energy U in Equation (34) can be rewritten for AFG-tapered microbeams as following

$$U^* = \frac{1}{2}\int_0^L \left[\left(E_{(x)} I_{(x)} + G_{(x)} A_{(x)} \left(2l_{0(x)}^2 + \frac{8}{15} l_{1(x)}^2 + l_{2(x)}^2 \right) \right) \left(\frac{d^2 w}{dx^2} \right)^2 + \left(G_{(x)} I_{(x)} \left(2l_{0(x)}^2 + \frac{4}{5} l_{1(x)}^2 \right) \right) \left(\frac{d^3 w}{dx^3} \right)^2 \right] dx \tag{40}$$

4. Application of Rayleigh–Ritz Method

The total potential energy of the AFG-tapered microbeam can be expressed as

$$\Pi = U^* - W \tag{41}$$

where U^* is the strain energy of the AFG-tapered microbeam and W is the work done by axial compressive load as

$$W = \frac{P}{2}\int_0^L \left(\frac{dw}{dx} \right)^2 dx \tag{42}$$

where P is the axial compressive load. The total potential energy of the AFG-tapered microbeam is written by using Equations (40) and (42) in Equation (41) as

$$\Pi = \frac{1}{2}\int_0^L \left[\left(E_{(x)} I_{(x)} + G_{(x)} A_{(x)} \left(2l_{0(x)}^2 + \frac{8}{15} l_{1(x)}^2 + l_{2(x)}^2 \right) \right) \left(\frac{d^2 w}{dx^2} \right)^2 + \left(G_{(x)} I_{(x)} \left(2l_{0(x)}^2 + \frac{4}{5} l_{1(x)}^2 \right) \right) \left(\frac{d^3 w}{dx^3} \right)^2 \right] dx - \frac{P}{2}\int_0^L \left(\frac{dw}{dx} \right)^2 dx \tag{43}$$

Utilizing Rayleigh–Ritz method with assumed trial function, $w(x)$ can be defined as

$$w(x) = \sum_{i=1}^{N} a_i \varphi_i(x) \tag{44}$$

where a_i are the constants and $\varphi_i(x)$ is the admissible function which is necessary to satisfy only the geometric (essential) boundary conditions. The geometric boundary conditions of clamped and pinned ends for classical case are

$$\text{Clamped (C)}: \; w = 0, \; \frac{dw}{dx} = 0 \tag{45}$$

$$\text{Pinned (P)}: \; w = 0 \tag{46}$$

For nonclassical boundary conditions, two enable boundary conditions are possible at fixed ends as [5,15]

$$M_{nc} = \frac{d^3 w}{dx^3} = 0 \tag{47}$$

$$\frac{d^2 w}{dx^2} = 0 \tag{48}$$

In the present study, two admissible functions are chosen to be dependent on cantilever (clamped-free) and propped cantilever (clamped-pinned) microbeams as following

$$\text{Cantilever (BC1)}: \; \varphi_i^1(x) = (x)^{i+1}, \; i = 1, 2, \ldots, 10 \tag{49}$$

$$\text{Cantilever (BC2)}: \; \varphi_i^2(x) = (x)^{i+2}, \; i = 1, 2, \ldots, 10 \tag{50}$$

$$\text{Propped cantilever (BC1)}: \; \varphi_i^1(x) = (x)^{i+1}(L - x), \; i = 1, 2, \ldots, 10 \tag{51}$$

$$\text{Propped cantilever (BC2)}: \; \varphi_i^2(x) = (x)^{i+2}(L - x), \; i = 1, 2, \ldots, 10 \tag{52}$$

The stationary points of the total potential energy are the solutions which satisfy equilibrium as

$$\frac{\partial \Pi}{\partial a_i} = 0,\ i = 1, 2, \ldots, 10 \tag{53}$$

For a non-trivial solution, the determinant of the coefficient matrix must be equal to zero. Consequently, ten roots of this eigenvalue problem can be assessed and the smallest of them indicates the critical buckling load.

For illustration purposes, the solution of Equation (53) is presented for homogeneous uniform cantilever beams with $i = 2$. In this case, $w(x)$ can be written according to Equations (44) and (49) as

$$w(x) = a_1 x^2 + a_2 x^3 \tag{54}$$

The total potential energy of a homogeneous uniform beam can be expressed as

$$\Pi = \frac{1}{2}\int_0^L \left[EI\left(\frac{d^2 w}{dx^2}\right)^2 - P\left(\frac{dw}{dx}\right)^2 \right] dx \tag{55}$$

Substituting Equation (54) in Equation (55) yields

$$\begin{array}{c} \Pi = \frac{1}{2}\int_0^L \left[EI(2a_1 + 6a_2 x)^2 - P\left(2a_1 x + 3a_2 x^2\right)^2 \right] dx \\ = 2EIL\left(a_1^2 + 3a_1 a_2 L + 3a_2^2 L^2\right) - \frac{PL^3}{30}\left(20a_1^2 + 45a_1 a_2 L + 27a_2^2 L^2\right) \end{array} \tag{56}$$

Use of Equation (56) in Equation (53) gives the following relations

$$\frac{\partial \Pi}{\partial a_1} = EIL(4a_1 + 6a_2 L) - PL^3\left(\frac{4}{3}a_1 + \frac{3}{2}a_2 L\right) = 0 \tag{57}$$

$$\frac{\partial \Pi}{\partial a_2} = EIL\left(6a_1 L + 12a_2 L^2\right) - PL^3\left(\frac{3}{2}a_1 L + \frac{9}{5}a_2 L^2\right) = 0 \tag{58}$$

Equations (57) and (58) can be written in matrix form as

$$\begin{bmatrix} K_{11} & K_{12} \\ K_{21} & K_{22} \end{bmatrix} \begin{Bmatrix} a_1 \\ a_2 \end{Bmatrix} = 0 \tag{59}$$

where

$$K_{11} = 4L\left(EI - \frac{PL^2}{3}\right),\ K_{12} = K_{21} = 3L^2\left(2EI - \frac{PL^2}{2}\right),\ K_{22} = 3L^3\left(4EI - \frac{3PL^2}{5}\right) \tag{60}$$

Two dimensionless roots are obtained by equaling to zero the determinant of the coefficient matrix in Equation (59) and multiplying $\frac{L^2}{EI}$ as

$$\lambda_1 = 2.4860 \text{ and } \lambda_2 = 32.1807 \tag{61}$$

The smallest root (λ_1) indicates the critical buckling load. It is notable that Equation (56) is written for $i = 10$ as

$$\begin{bmatrix} K_{11} & \cdots & K\_110 \\ \vdots & \ddots & \vdots \\ K_{101} & \cdots & K_{1010} \end{bmatrix} \begin{Bmatrix} a_1 \\ \vdots \\ a_{10} \end{Bmatrix} = 0 \tag{62}$$

Similarly, ten roots can be assessed and the smallest of them indicates the critical buckling load.

5. Results and Discussion

First, in order to prove the validity and accuracy of the current results, comparisons and convergences for the dimensionless classical critical buckling loads of tapered homoge-

neous columns are presented in Tables 1 and 2 for various taper ratios and cantilever and propped cantilever microbeams, respectively. It is revealed from the table that the exact and present results agree very well for two boundary conditions and all taper ratios.

Table 1. Comparison and convergence of dimensionless critical buckling loads for homogeneous tapered cantilever microbeams ($l_0 = l_1 = l_2 = 0$).

Taper Ratio, α	Present					Exact
	$N = 2$	$N = 4$	$N = 6$	$N = 8$	$N = 10$	[49]
0	2.4860	2.4674	2.4674	2.4674	2.4674	2.467
0.1	2.4165	2.3928	2.3928	2.3928	2.3928	2.393
0.3	2.2702	2.2351	2.2351	2.2351	2.2351	2.235
0.5	2.1078	2.0621	2.0621	2.0621	2.0621	2.062
0.7	1.9140	1.8655	1.8653	1.8653	1.8653	1.865
0.9	1.6462	1.6229	1.6212	1.6211	1.6211	1.621

Table 2. Comparison and convergence of dimensionless critical buckling loads for homogeneous tapered propped cantilever microbeams ($l_0 = l_1 = l_2 = 0$).

Taper Ratio, α	Present					Exact
	$N = 2$	$N = 4$	$N = 6$	$N = 8$	$N = 10$	[49]
0	20.9187	20.1943	20.1907	20.1907	20.1907	20.1907
0.1	19.9908	19.1736	19.1686	19.1686	19.1686	19.17
0.3	18.0621	17.0426	17.0354	17.0353	17.0353	17.03
0.5	15.9584	14.7452	14.7394	14.7394	14.7394	14.74
0.7	13.4459	12.1775	12.1773	12.1772	12.1772	12.18
0.9	9.7113	9.0608	9.0307	9.0295	9.0294	9.029

Because the comparative results above are based on classical theory, another comparison of size-dependent dimensionless critical buckling loads for homogeneous tapered cantilever microbeams made of epoxy is given in Table 3. For the purpose of comparison, the material and geometric properties are used as indicated in Ref. [40] for this table only. It is observed that there is an excellent agreement between the compared results.

Table 3. Comparison of size-dependent dimensionless critical buckling loads for tapered cantilever epoxy microbeams ($l_0 = l_1 = l_2 = h_1$).

Taper Ratio, α	BC1		BC2	
	Present	[40]	Present	[40]
0	40.38752	40.3875	41.52736	41.5274
0.2	35.20555	35.2055	36.04467	36.0447
0.4	29.81004	29.8100	30.38676	30.3868
0.6	24.04835	24.0483	24.40082	24.4008
0.8	17.51253	17.5125	17.67871	17.6787

Tables 4 and 5 show the variation of dimensionless critical buckling loads for AFG-tapered microbeams for various gradient indices. It is assumed in the analysis that $E_L = 2E_R$, $l_L = 2l_R$ and $v_L = v_R = 0.3$. The tables demonstrate that an increase in the material property gradient index gives rise to an increment in the critical buckling loads. Furthermore, it can be said that the critical buckling loads obtained based on SGT are always bigger than those evaluated by CT. In addition, it is seen from these two tables that the critical buckling loads for $\alpha = 0.25$ are greater than those for $\alpha = 0.75$. Moreover, it is notable that the critical buckling loads obtained for BC2 are larger than those for BC1 and that this situation is more prominent for propped cantilever microbeams.

Table 4. Dimensionless buckling loads for nonhomogeneous tapered microbeams for various gradient indices (α = 0.25, $l_L = h_1$).

n	Cantilever			Propped Cantilever		
	CT	SGT-BC1	SGT-BC2	CT	SGT-BC1	SGT-BC2
0	2.2757	11.5570	11.8369	17.5814	89.5126	91.6124
0.5	3.2955	29.7361	30.0206	22.8377	175.9789	178.2837
1	3.7659	43.0086	43.5267	25.4402	232.7055	236.3154
2	4.1851	59.4975	60.5222	28.5113	314.3887	319.9357
10	4.5350	77.8720	79.8187	34.3698	564.3991	577.0945

Table 5. Dimensionless buckling loads for nonhomogeneous tapered microbeams for various gradient indices (α = 0.75, $l_L = h_1$).

n	Cantilever			Propped Cantilever		
	CT	SGT-BC1	SGT-BC2	CT	SGT-BC1	SGT-BC2
0	1.8104	9.1937	9.3599	11.4694	58.3994	59.4905
0.5	2.5358	21.4730	21.6085	14.5021	107.0497	108.1194
1	2.8923	30.5769	30.8118	16.0267	138.5213	140.1774
2	3.2404	43.0156	43.4926	17.8791	183.6129	186.1580
10	3.5961	62.2555	62.3944	22.0821	348.4897	354.3562

Variations of dimensionless buckling loads for cantilever and propped cantilever AFG-tapered microbeams with respect to h_1/l for different taper ratios are illustrated in Figures 2 and 3, respectively. It can be seen from these figures that size-dependent buckling loads decrease by increasing h_1/l_L, approaching classical results. Moreover, it is observed that the critical buckling loads for $\alpha = 0.3$ are greater than those for $\alpha = 0.6$.

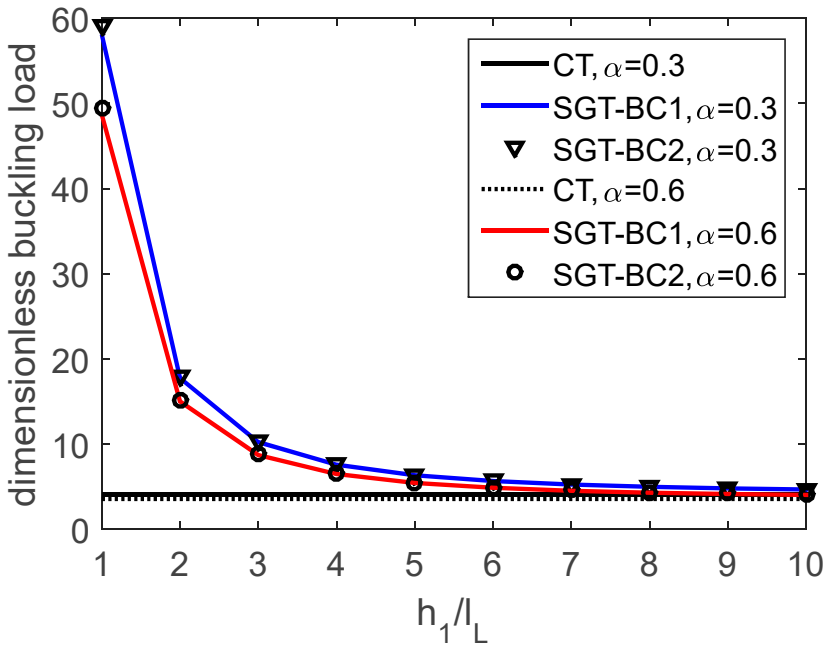

Figure 2. Variation of dimensionless buckling load for cantilever microbeams with respect to h_1/l_L for different taper ratios ($n = 2$).

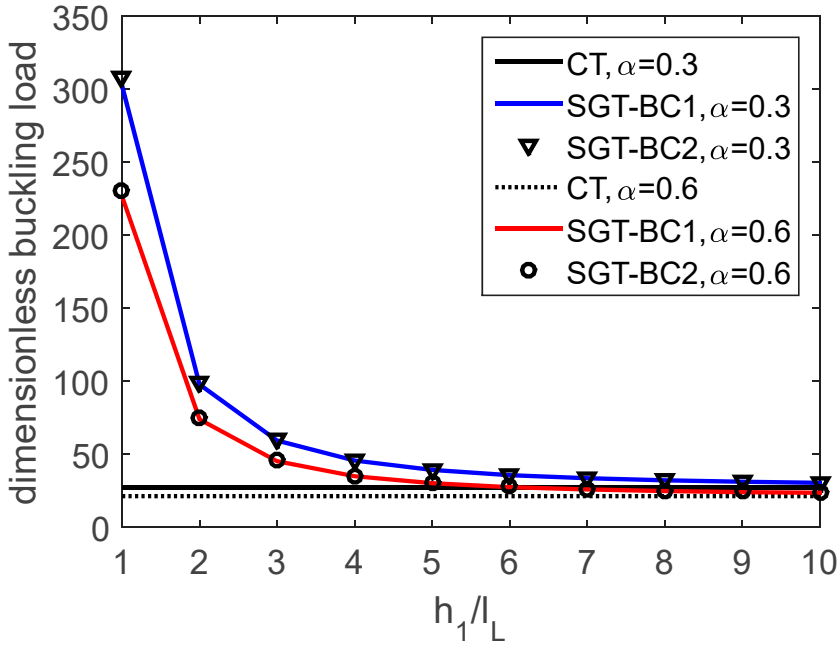

Figure 3. Variation of dimensionless buckling load for propped cantilever microbeams with respect to h_1/l_L for different taper ratios ($n = 2$).

Influences of nonclassical boundary conditions on the size-dependent dimensionless buckling loads with respect to various taper ratios for cantilever and propped cantilever microbeams are depicted in Figures 4 and 5, respectively. It can be found from the figures that a decrement occurs in the buckling loads when increasing the taper ratio. Furthermore, the difference between the critical buckling loads evaluated for BC1 and BC2 is more evident for smaller taper ratios, especially for a uniform cross-section when $\alpha = 0$. This difference diminishes by increasing the taper ratio.

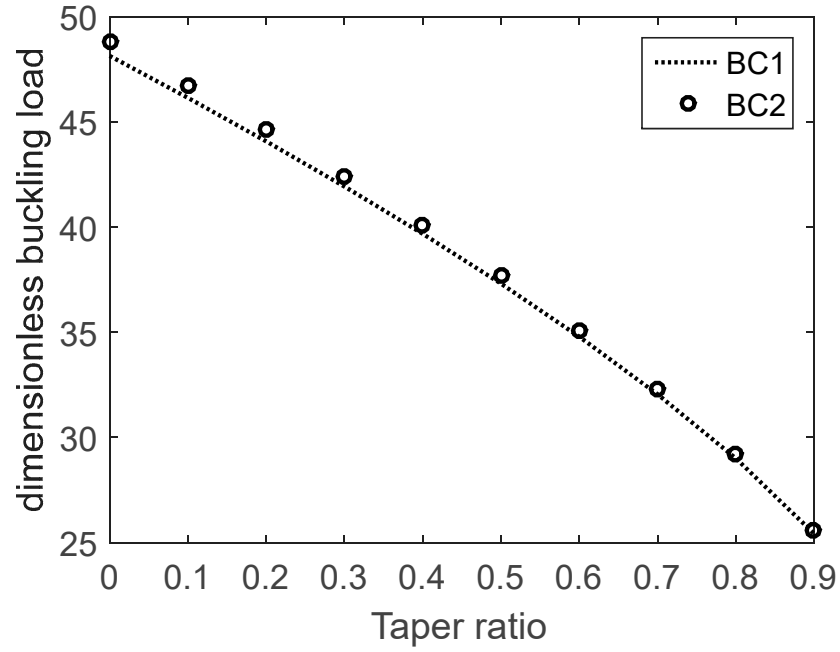

Figure 4. Effects of nonclassical boundary conditions on the dimensionless buckling load of cantilever microbeams corresponding to various taper ratios ($n = 1$, $l_L = h_1$).

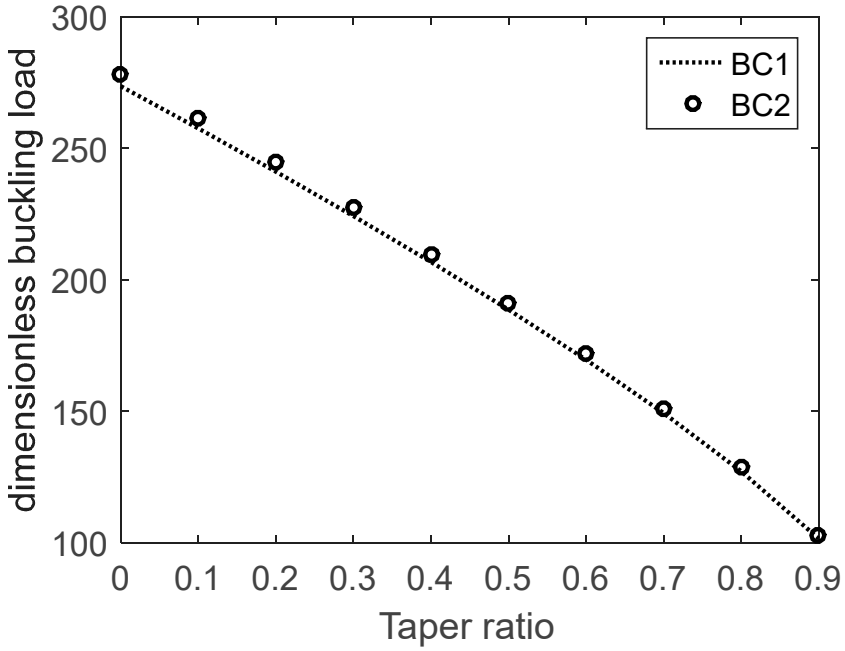

Figure 5. Effects of nonclassical boundary conditions on the dimensionless buckling load of propped cantilever microbeams corresponding to various taper ratios ($n = 1$, $l_L = h_1$).

6. Conclusions

In this study, buckling behavior of axially functionally graded non-prismatic microbeams is examined via modified strain gradient theory. The Rayleigh–Ritz method is implemented to solve the problem with cantilever and propped cantilever microbeams for various taper ratios and gradient indices. A detailed parametric study is performed to investigate the influences of taper ratio, material gradient index, length scale parameter, and boundary conditions on the critical buckling loads. It can be concluded that size effect is more important for smaller h_1/l_L. Futhermore, non-classical boundary conditions are more effective for propped cantilever microbeams than cantilever ones.

Author Contributions: Conceptualization, B.A. and Ö.C.; methodology, B.A.; software, B.A.; validation, B.A.; formal analysis, B.A.; investigation, B.A.; resources, B.A.; data curation, B.A.; writing—original draft preparation, B.A.; writing—review and editing, Ö.C.; visualization, B.A.; supervision, Ö.C.; project administration, Ö.C.; funding acquisition, Ö.C. All authors have read and agreed to the published version of the manuscript.

Funding: This research received no external funding.

Data Availability Statement: Not applicable.

Conflicts of Interest: The authors declare no conflict of interest.

References

1. Koizumi, M.; Niino, M. Overview of Fgm Research in Japan. *Mrs. Bull.* **1995**, *20*, 19–21. [CrossRef]
2. Witvrouw, A.; Mehta, A. The use of functionally graded poly-SiGe layers for MEMS applications. *Mater. Sci. Forum* **2005**, *492–493*, 255–260. [CrossRef]
3. Mohammadi-Alasti, B.; Rezazadeh, G.; Borgheei, A.M.; Minaei, S.; Habibifar, R. On the mechanical behavior of a functionally graded micro-beam subjected to a thermal moment and nonlinear electrostatic pressure. *Compos. Struct.* **2011**, *93*, 1516–1525. [CrossRef]
4. Wei, Q.F.; Wang, X.Q.; Gao, W.D. AFM and ESEM characterisation of functionally nanostructured fibres. *Appl. Surf. Sci.* **2004**, *236*, 456–460. [CrossRef]
5. Lam, D.C.C.; Yang, F.; Chong, A.C.M.; Wang, J.; Tong, P. Experiments and theory in strain gradient elasticity. *J. Mech. Phys. Solids* **2003**, *51*, 1477–1508. [CrossRef]
6. Lei, J.; He, Y.M.; Guo, S.; Li, Z.K.; Liu, D.B. Size-dependent vibration of nickel cantilever microbeams: Experiment and gradient elasticity. *Aip. Adv.* **2016**, *6*, 105202. [CrossRef]

7. Xie, Y.Y.; Lei, J.; Guo, S.; Han, S.H.; Ruan, J.; He, Y.M. Size-dependent vibration of multi-scale sandwich micro-beams: An experimental study and theoretical analysis. *Thin Wall Struct.* **2022**, *175*, 109115. [CrossRef]
8. Guo, S.; Xie, Y.Y.; Lei, J.; Han, S.H.; Liu, D.B.; He, Y.M. Coupled effect of specimen size and grain size on the stress relaxation of micron-sized copper wires. *J. Mater. Sci.* **2022**, *57*, 18655–18668. [CrossRef]
9. Yang, H.; Abali, B.E.; Timofeev, D.; Müller, W.H. Determination of metamaterial parameters by means of a homogenization approach based on asymptotic analysis. *Continuum Mech. Thermodyn.* **2020**, *32*, 1251–1270. [CrossRef]
10. Barchiesi, E.; dell'Isola, F.; Hild, F. On the validation of homogenized modeling for bi-pantographic metamaterials via digital image correlation. *Int. J. Solids Struct.* **2021**, *208*, 49–62. [CrossRef]
11. Placidi, L.; Andreaus, U.; Corte, A.D.; Lekszycki, T. Gedanken experiments for the determination of two-dimensional linear second gradient elasticity coefficients. *Z. Angew. Math. Phys.* **2015**, *66*, 3699–3725. [CrossRef]
12. Yang, H.; Timofeev, D.; Abali, B.E.; Li, B.; Müller, W.H. Verification of strain gradient elasticity computation by analytical solutions. *Z. Angew. Math. Mech.* **2021**, *101*, e202100023. [CrossRef]
13. Roudbari, M.A.; Jorshari, T.D.; Lu, C.F.; Ansari, R.; Kouzani, A.Z.; Amabili, M. A review of size-dependent continuum mechanics models for micro- and nano-structures. *Thin Wall Struct.* **2022**, *170*, 108562. [CrossRef]
14. Thai, H.T.; Vo, T.P.; Nguyen, T.K.; Kim, S.E. A review of continuum mechanics models for size-dependent analysis of beams and plates. *Compos. Struct.* **2017**, *177*, 196–219. [CrossRef]
15. Akgoz, B.; Civalek, O. Buckling analysis of functionally graded microbeams based on the strain gradient theory. *Acta Mech.* **2013**, *224*, 2185–2201. [CrossRef]
16. Akgoz, B.; Civalek, O. A size-dependent shear deformation beam model based on the strain gradient elasticity theory. *Int. J. Eng. Sci.* **2013**, *70*, 1–14. [CrossRef]
17. Akgoz, B.; Civalek, O. Thermo-mechanical buckling behavior of functionally graded microbeams embedded in elastic medium. *Int. J. Eng. Sci.* **2014**, *85*, 90–104. [CrossRef]
18. Akgoz, B.; Civalek, O. Longitudinal vibration analysis for microbars based on strain gradient elasticity theory. *J. Vib. Control* **2014**, *20*, 606–616. [CrossRef]
19. Akgoz, B.; Civalek, O. A novel microstructure-dependent shear deformable beam model. *Int. J. Mech. Sci.* **2015**, *99*, 10–20. [CrossRef]
20. Akgoz, B.; Civalek, O. Bending analysis of embedded carbon nanotubes resting on an elastic foundation using strain gradient theory. *Acta Astronaut.* **2016**, *119*, 1–12. [CrossRef]
21. Barretta, R.; Fabbrocino, F.; Luciano, R.; de Sciarra, F.M.; Ruta, G. Buckling loads of nano-beams in stress-driven nonlocal elasticity. *Mech. Adv. Mater. Struct.* **2020**, *27*, 869–875. [CrossRef]
22. Barretta, R.; Faghidian, S.A.; Luciano, R.; Medaglia, C.M.; Penna, R. Free vibrations of FG elastic Timoshenko nano-beams by strain gradient and stress-driven nonlocal models. *Compos. Part B-Eng.* **2018**, *154*, 20–32. [CrossRef]
23. Barretta, R.; Feo, L.; Luciano, R.; de Sciarra, F.M.; Penna, R. Functionally graded Timoshenko nanobeams: A novel nonlocal gradient formulation. *Compos. Part B-Eng.* **2016**, *100*, 208–219. [CrossRef]
24. Ghandourah, E.E.; Daikh, A.A.; Alhawsawi, A.M.; Fallatah, O.A.; Eltaher, M.A. Bending and Buckling of FG-GRNC Lamineted Plates via Quasi-3D Nonlocal Strain Gradient Theory. *Mathematics* **2022**, *10*, 1321. [CrossRef]
25. Ma, H.M.; Gao, X.L.; Reddy, J.N. A microstructure-dependent Timoshenko beam model based on a modified couple stress theory. *J. Mech. Phys. Solids* **2008**, *56*, 3379–3391. [CrossRef]
26. Numanoglu, H.M.; Ersoy, H.; Akgoz, B.; Civalek, O. A new eigenvalue problem solver for thermo-mechanical vibration of Timoshenko nanobeams by an innovative nonlocal finite element method. *Math. Method Appl. Sci.* **2022**, *45*, 2592–2614. [CrossRef]
27. Pinnola, F.P.; Barretta, R.; de Sciarra, F.M.; Pirrotta, A. Analytical Solutions of Viscoelastic Nonlocal Timoshenko Beams. *Mathematics* **2022**, *10*, 477. [CrossRef]
28. Reddy, J.N. Nonlocal theories for bending, buckling and vibration of beams. *Int. J. Eng. Sci.* **2007**, *45*, 288–307. [CrossRef]
29. Reddy, J.N. Microstructure-dependent couple stress theories of functionally graded beams. *J. Mech. Phys. Solids* **2011**, *59*, 2382–2399. [CrossRef]
30. Zenkour, A.M.; Hafed, Z.S.; Radwan, A.F. Bending Analysis of Functionally Graded Nanoscale Plates by Using Nonlocal Mixed Variational Formula. *Mathematics* **2020**, *8*, 1162. [CrossRef]
31. Rajasekaran, S. Differential transformation and differential quadrature methods for centrifugally stiffened axially functionally graded tapered beams. *Int. J. Mech. Sci.* **2013**, *74*, 15–31. [CrossRef]
32. Rajasekaran, S. Buckling and vibration of axially functionally graded nonuniform beams using differential transformation based dynamic stiffness approach. *Meccanica* **2013**, *48*, 1053–1070. [CrossRef]
33. Lee, J.K.; Lee, B.K. Free vibration and buckling of tapered columns made of axially functionally graded materials. *Appl. Math. Model.* **2019**, *75*, 73–87. [CrossRef]
34. Huang, Y.; Yang, L.E.; Luo, Q.Z. Free vibration of axially functionally graded Timoshenko beams with non-uniform cross-section. *Compos. Part B-Eng.* **2013**, *45*, 1493–1498. [CrossRef]
35. Boutahar, Y.; Lebaal, N.; Bassir, D. A Refined Theory for Bending Vibratory Analysis of Thick Functionally Graded Beams. *Mathematics* **2021**, *9*, 1422. [CrossRef]
36. Ge, R.Y.; Liu, F.; Wang, C.; Ma, L.L.; Wang, J.P. Calculation of Critical Load of Axially Functionally Graded and Variable Cross-Section Timoshenko Beams by Using Interpolating Matrix Method. *Mathematics* **2022**, *10*, 2350. [CrossRef]

37. Mahmoud, M.A. Natural frequency of axially functionally graded, tapered cantilever beams with tip masses. *Eng. Struct.* **2019**, *187*, 34–42. [CrossRef]
38. Mirjavadi, S.S.; Matin, A.; Shafiei, N.; Rabby, S.; Afshari, B.M. Thermal buckling behavior of two-dimensional imperfect functionally graded microscale-tapered porous beam. *J. Therm. Stresses* **2017**, *40*, 1201–1214. [CrossRef]
39. Singh, R.; Sharma, P. Vibration analysis of an axially functionally graded material non-prismatic beam under axial thermal variation in humid environment. *J. Vib. Control* **2022**, *28*, 3608–3621. [CrossRef]
40. Akgoz, B.; Civalek, O. Buckling analysis of linearly tapered micro-columns based on strain gradient elasticity. *Struct. Eng. Mech.* **2013**, *48*, 195–205. [CrossRef]
41. Akgoz, B. Static stability analysis of axially functionally graded tapered micro columns with different boundary conditions. *Steel Compos. Struct.* **2019**, *33*, 133–142.
42. Ebrahimi, F.; Barati, M.R. Buckling analysis of nonlocal strain gradient axially functionally graded nanobeams resting on variable elastic medium. *Proc. Inst. Mech. Eng. Part C J. Mech. Eng. Sci.* **2018**, *232*, 2067–2078. [CrossRef]
43. Haddad, S.; Baghani, M.; Zakerzadeh, M.R. Size dependent analysis of tapered FG micro-bridge based on a 3D beam theory. *Sci. Iran* **2020**, *27*, 2889–2901. [CrossRef]
44. Mohammadimehr, M.; Alimirzaei, S. Buckling and free vibration analysis of tapered FG-CNTRC micro Reddy beam under longitudinal magnetic field using FEM. *Smart Struct. Syst.* **2017**, *19*, 309–322. [CrossRef]
45. Mohammadimehr, M.; Monajemi, A.A.; Moradi, M. Vibration analysis of viscoelastic tapered micro-rod based on strain gradient theory resting on visco-pasternak foundation using DQM. *J. Mech. Sci. Technol.* **2015**, *29*, 2297–2305. [CrossRef]
46. Shafiei, N.; Mousavi, A.; Ghadiri, M. On size-dependent nonlinear vibration of porous and imperfect functionally graded tapered microbeams. *Int. J. Eng. Sci.* **2016**, *106*, 42–56. [CrossRef]
47. Shafiei, N.; Kazemi, M. Buckling analysis on the bi-dimensional functionally graded porous tapered nano-/micro-scale beams. *Aerosp. Sci. Technol.* **2017**, *66*, 1–11. [CrossRef]
48. Shafiei, N.; Ghadiri, M.; Mahinzare, M. Flapwise bending vibration analysis of rotary tapered functionally graded nanobeam in thermal environment. *Mech. Adv. Mater. Struct.* **2019**, *26*, 139–155. [CrossRef]
49. Wang, C.M.; Wang, C.Y.; Reddy, J.N. *Exact Solutions for Buckling of Structural Members*, 1st ed.; CRC Press: Boca Raton, FL, USA, 2004.